BIOMECHANICAL INTERPRETATION OF THE REFLECTED WAVES IN THE INTRAORGAN BEDS: A NOVEL METHOD OF DIAGNOSTICS

N.N. Kizilova*, H.N. Philippova*, O.K. Zenin**

*Department of Theoretical Mechanics, Kharkov National University, Kharkov, Ukraine
**Donetsk National Medical University, Donetsk, Ukraine

nnk_@.bk.ru

Abstract: Pulse wave propagation in the models of the intraorgan arterial beds is investigated. For the beds without anastomoses the self-similar tree-like branching systems of viscoelastic tubes is considered whereas for the beds with loops the topology and geometry of the vasculature is measured on plastic casts of the arterial vasculatures. The stationary Poiseuille flow in each tube and the Womersley model of the time-dependent flow in a thick-walled distensible tube is used for calculations of the hydraulic impedance and wave input admittance of the vasculatures. It is shown that the resonant harmonics of the input admittance, wave intensity analysis and the pressure-flow loops can be used in medical diagnostics on the pressure and flow curves measured by the ultrasound devices at an arbitrary cross-section of the feeding artery of the intraorgan vasculature. The biomechanical interpretation of the pathological variations of the parameters is presented.

Introduction

Mathematical models of steady flow and wave propagation in the systems of distensible tubes have been developed as the models of blood circulation [1-5]. Blood flow in the intraorgan vasculatures have been investigated basing on the fractal tree-like systems of tubes [6-8] but validity of the approach has been analyzed for the pulmonary arterial tree mostly [9]. Recent investigations revealed the new data concerning the structure of coronary arterial beds [10] and branching fractal networks [6-8], the differences in hydraulic and wave properties of vasculatures with anastomoses and without them [11-13], resonant properties of the arterial beds of different inner organs [14-16]. The data can be used for novel methods of pulse wave diagnostics elaboration as well as biomechanical interpretation of traditional pulse diagnostics of oriental medicine.

Here the models of the intraorgan vasculatures based on the morphometric data on geometry and topology of real arterial beds of the main inner organs are presented.

Materials and Methods

Hydrodynamic properties of the branching systems of tubes are characterized by the hydraulic impedance $Z = P/Q$ and input (wave) impedance $Z_{in} = P_a / Q_a$ where P,Q are average pressure and flow rate, P_a, Q_a are pressure and volumetric rate amplitudes at the inlet of the feeding artery. When the input signal $P(t)$ (or $Q(t)$) at the inlet of the feeding artery is considered as Fourier series, the spectra of the input impedance $Z_{in}(n)$ where n is the number of harmonics can be considered. The values $Z, Z_{in}(n)$ can be calculated for an arbitrary tree-like system of the tubes by consequent calculations of the impedances of the tubes which are in parallel and series connection [17]. The data on lengths, diameters, wall thickness and elasticity have to be used for calculations. The detailed morphometric data include several thousand numbers obtained by plastic casts of the arterial bed of an individual [5]. Real vasculatures of different individuals undergo numerous variations on topology and geometry. In that way modelling of the arterial beds using some regularity in construction of the arterial systems is an important problem for developing the general models which are representative for the vasculature of a given inner organ and insensitive to possible individual variations and for using them in clinical applications and medical diagnostics.

In most cases the feeding arteries of the vasculatures are accessible for the non-invasive measurements. The volumetric rate $Q(t)$, linear velocity $U(t)$ and diameter oscillations $d(t)$ can be measured at the cross-section of the feeding artery by ultrasound devices. Pressure curves $P(t)$ can be restored by the curves $d(t)$ with wall tracing techniques. The measured signals $P(t)$, $U(t)$ can be used for separation of the travelling waves into their forward P^+, U^+ and backward P^-, U^- components [18]. The curves $P^-(t), U^-(t)$ contain information about flow conditions in the organ that can be used in clinical diagnostics after the biomechanical interpretation of the wave parameters is carried out.

The general relationships between the lengths L_j and diameters d_j of the consecutive vessels and between the diameters $d_{0-2,j}$ of the vessels in each

ISSN: 1727-1983

bifurcation have been obtained as statistical regularities in numerous measurements and experiments [19-22]. Here we introduce the relationships as follows: $d_{1j}=\xi d_{0j}/\sqrt[\gamma]{1+\xi^{\gamma}}$, $R_{2j}=R_{0j}/\sqrt[\gamma]{1+\xi^{\gamma}}$, $L_j=\alpha d_j^{\beta}$, where $\xi=min\{d_{1j},d_{2j}\}/max\{d_{1j},d_{2j}\}$ is the branching asymmetry coefficient, $\gamma=3$ (Murray's law), α,β are constant for a given vasculature [9]. The arbitrary deviations of L_j and d_j within the physiological range ($\pm 10\%$ for d_j and $\pm 30\%$ for L_j) have been introduced for investigation of the role of individual variations in geometry of the arterial beds.

The Poiseuille flow of a viscous fluid through the rigid tube is considered as a model of steady blood flow. Here $Z_j=k_jL_jR_j^{-4}$ is the hydraulic impedance of the j-th tube, where $k_j=8\pi/\mu(R_j)$, μ is blood viscosity and the dependence $\mu(R_j)$ corresponds to Fahreus-Lindquist effect. In the wave motion the values Z_j correspond to the harmonics n=0 as well. The Womersley model of the time-dependent blood motion of a viscous incompressible liquid in the thick-walled viscoelastic cylindrical tube gives the following relations for the pressure P_j and volumetric rate Q_j in the j-th tube (taking into consideration pulse wave reflections at the end of each vessel in the system):

$$\begin{aligned} P_i &= P_i^0\left(e^{i\omega(t-x_i/c_i)}+\Gamma_i e^{i\omega(t+(x_i-2L_i)/c_i)}\right) \\ Q_i &= Y_i^0P_i^0\left(e^{i\omega(t-x_i/c_i)}-\Gamma_i e^{i\omega(t+(x_i-2L_i)/c_i)}\right) \end{aligned} \qquad (2)$$

where $P_j^0=P_j\big|_{x_j=0}$, $\alpha_j=R_j\sqrt{\omega\rho/\mu}$, $i=\sqrt{-1}$, $F_j=2J_1(\beta_j)/(\beta_jJ_0(\beta_j))$, $\beta_j=\alpha_j(-1)^{3/4}$, $c_j=\left(E_jh_j(1-F_{01})e^{i\theta}/(2\rho R_j(1-\sigma_j^2))\right)^{1/2}$ is the wave velocity, x_i is the axial coordinate, $Y_j^0=(\pi d_j^2)/(4\rho c_j)$ is the characteristic admittance, Γ_j is reflection coefficient, E_j,σ_j,θ are elasticity modulus, Poisson's ratio and viscosity of the wall material, ρ is blood density, h_j is the wall thickness.

For the models of tree-like branching systems and real vasculatures without anastomoses the total values Z and Z_{in} have been calculated starting from the last order tubes [17]. For the models and vasculatures with anastomoses the pressure and flow continuity conditions at each bifurcation together with relations (1)-(2) for each tube give the nonlinear system of algebraic equations with complex coefficients for P_j^0 and Γ_j [11]. The numerical solution of the system has been obtained by modified Newton's method.

In that way the pressure and flow curves $P(t)$, $U(t)$ in the feeding arteries of the models can be computed. The waves $P^{\pm},U^{\pm}$ and intensities $I^{\pm}$ of the forward and backward components are calculated as follows [18]:

$$P^{\pm}=(P\pm\rho cU)/2,$$

$$U^{\pm}=(\rho cU\pm P)/2\rho c$$

$$I^{\pm}(t)=\pm\frac{1}{4\rho c}\int(dP\pm\rho cdU)^2dt$$

Two types of vasculatures have been considered: tree-like systems for the coronary, brain, liver and kidney arterial beds (Figure 1a) and the systems with numerous loops for the large and small intestine (Figure 1b). Geometrical parameters of the vasculatures have been measured on plastic casts of the arterial beds of the main inner organs of a human.

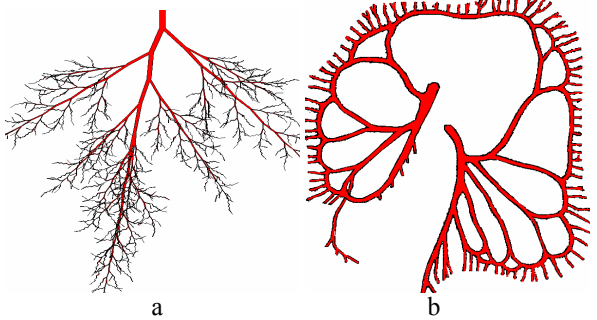

a b

Figure 1: Intraorgan vasculatures of the spleen (a) and large intestine (b) of a human

Results and discussions

The parameters $h_j=\lambda d_j$, $\lambda=0.14-0.2$, $E=(6-9)\cdot10^5$ Pa and $E=(1-2)\cdot10^6$ P for the arteries of elastic and muscle types respectively have been used for calculations. The scatter of distances from the inlet of the feeding artery monotonically increases while ξ decreases. For the symmetrical trees this scatter is relatively small and they will exhibit acute resonant properties because of quite equal times of the backward pulse waves travelling from different bifurcations with the same branching orders. This means that the results for asymmetric trees are more realistic.

The dependence $Y^*(f)$, where $Y^*=Y_{in}/Y_0$, $Y_{in}=Z_{in}^{-1}$, f is the frequency is presented in Figure 2 for $L_0=0.2$ m, $d_0=0.03$ m, $\xi=0.2\div1$. The results of the calculations have shown that the influence of asymmetry in the average lengths of the arteries is negligible. All the changes are observed within the same harmonic and the variations do not exceed ±2 Hz.

For the pulse rate 60–75 1/min (the frequency of the main harmonic of the pulse wave $f_0=1-1.25$) the case depicted in Figure 3 corresponds to the resonance

ISSN: 1727-1983

at the 5-th harmonic. The first maximum of $Y^*(n)$ corresponds to the main resonant frequency of the intraorgan vasculature in terms [14-16]. At wide variation of ξ the main frequency variations do not exceed ± 6 Hz and correspond to the same harmonic. In this case the modulus of impedance reaches its maximum at the 4-th harmonic. In that way the correspondent component Q_4 of the flow rate penetrates in the vascular bed of the organ. Controversially, the modulus of impedance is minimal at the 7-th harmonic and so this component is mainly reflected by the vascular bed. The corresponding enhancement of the 7-th and weakening of the 4-th harmonics can be measured on any peripheral artery out-of the vascular tree of the organ with the ultrasound devices.

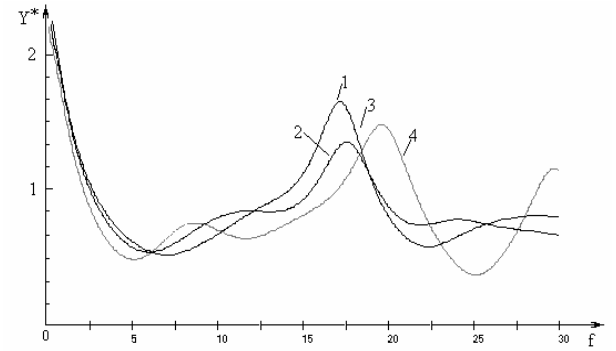

Figure 2: The dependence $Y^*(f)$ for $\xi = 0.2;0.4;0.6;0.8$ (numbers 1–4 respectively)

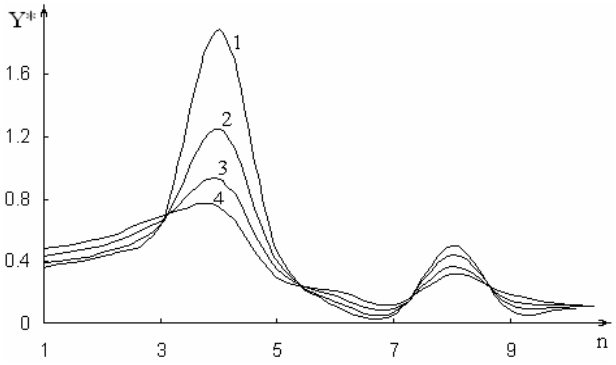

Figure 3: $Y^*(n)$ dependences for different reflection coefficient $\Gamma = 0.8;0.6;0.4;0.2$ (numbers 1-4)

The maximum $Y^*(n)$ corresponds to the 4-th ($f = 8-10$ Hz) and 8-th ($f = 128-160$ Hz) harmonic. According to the terminology [14–16], $i = 4;8$ are the main and addition resonant harmonics for the pulse diagnosis. The set of harmonics is the same for different values ξ, a, b and depends on the length L_0 of the feeding artery. This result conforms to the experimental observations [15].

The calculations revealed that even slight variations of the reflection coefficient led to noticeable changes in the amplitudes of the resonant harmonics. The real and image parts of the reflection coefficient $Re(\Gamma), Im(\Gamma)$ describe the resistive and capacitive properties of the microcirculatory bed. Thus, the individual scattering of geometrical parameters of the bed is insignificant, whereas any pathological variations caused considerable alterations of the amplitudes corresponding to the resonant harmonics of the effective admittance $Y^*(f)$.

When $\Gamma_j = 0$ pulse wave reflection at the bifurcation is absent (a well-matched junction). When $\Gamma_n = 1$ (reflection at the closed end of the tube) the relation (2) gives $Q_j = 0$ for the downstream blood flow. In real vascular beds the $|Re(\Gamma_n)| \le 0.2$ while in the extraorgan arteries $|Re(\Gamma_n)| \sim 0$ [23]. When we introduce the terminal admittance $Y_t = Y_0(1-\Gamma)/(1+\Gamma)$ we can investigate the pathological variations of the input impedance (admittance). When the capillary wall rigidity increases and for the patients with oedema, the value $Re(Y_t)$ increases, and by this way the amplitude of the backward pulse wave increases as well. The wall compliance increasing causes increasing $Im(Y_t)$. Thus, increasing $Re(Y_t)$ and decreasing $Im(Y_t)$ correspond to the redundancy syndrome in terms of the oriental medicine. Respectively, $Re(Y_t)$ decreasing and $Im(Y_t)$ increasing correspond to the insufficiency syndrome. The biomechanical interpretation of the reflection conditions in the downstream vasculature can be useful in the nosology of the oriental medicine [11].

Another useful result of the calculations is connected with interpretation of the forward-backward waves. In the vasculature with well-matched bifurcations the backward compressed wave may be produces by pathological occlusion of an artery or by increased wave reflection at the terminus (microcirculatory level). Extremes of the $I^{\pm}(t)$ curves correspond to the propagated and reflected waves and define the distances to the reflection sites. The influence of the stenosis (aneurisma) and the reflection coefficient at the terminal vessels can be distinguished. Shape of the waves $P^{\pm}(t), U^{\pm}(t)$ characterises the contribution of the multireflection into the signals. The surface area of the P(U) loops and the slope angle of its longer axis are important diagnostic characteristics of the intraorgan flow (Figure 4).

For the vasculatures with loops (Figure 1b) the comparative study of eight vasculatures with significant differences in topology, the number of the loops (n=14-22) and the terminal subtrees (n=83-108) has been carried out. The total volume of the main arteries V=12.98-15.88 cm^3 correlates ($R^2 = 0.98$) with the

ISSN: 1727-1983

average diameter $\langle d \rangle = (d_1 + d_2)/2$ of the feeding arteries with diameters $d_{1,2}$. Distribution of the flow rate Q between the terminal subtrees depends on the topology of the system and the length of the arterial segments in the loops (Figure 5). Compression of one of the branches of the feeding arteries (I-IV in fig.1a) leads to decreasing the flow rates in immediate proximity to the compressed segment at relatively constant blood flow in the other subtrees (Figure 5).

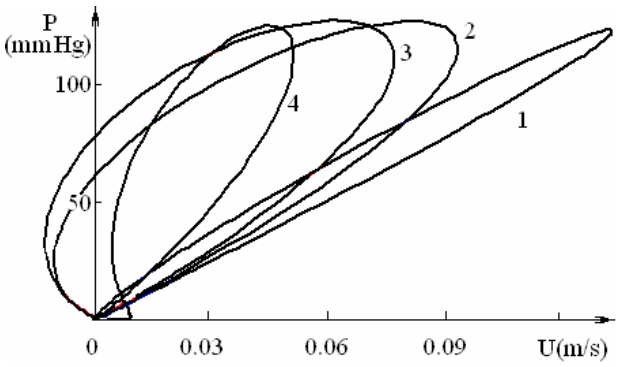

Figure 4: P(U) curves for the spleen arterial bed at $\Gamma = 0.2;0.4;0.6;0.8$ (numbers 1-4)

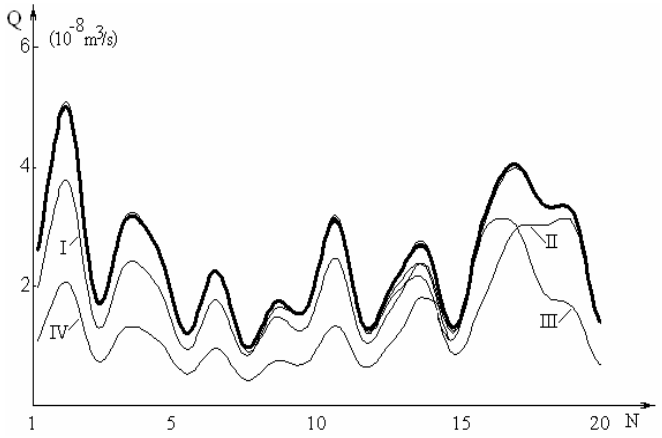

Figure 5. Flow rate distribution in the terminal elements in the normal state (solid line) and after compression of the segments I-IV

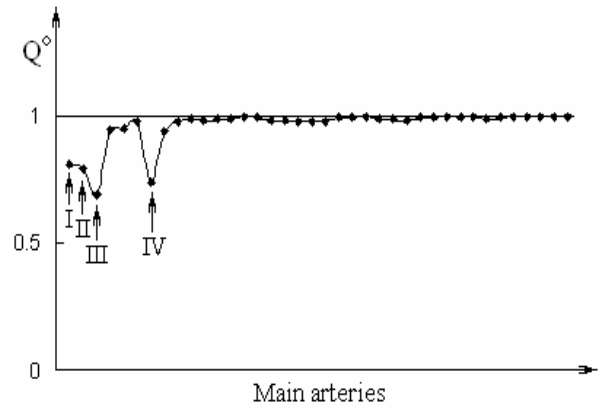

Figure 6. Dimensionless flow rate $Q^\circ = Q / Q_0$ in the vasculature after compression of the main arteries. Compression of the segments I-IV is marked by the arrows

Compression of the other arteries in the system leads to insignificant variations of the flow rate in the downstream loops only. For comparison the similar compression of any segment in a tree-like arterial system leads to interruption in blood flow in the downstream vasculature and ischemia. Variations of the total blood flow rate $Q = q_1 + q_2$ relative to the undisturbed state Q_0 are noticeable only for the cross-clamping of the main segments I-IV (Figure 6).

Occlusion of the vessels cause the most noticeable variations of the blood supply only in the relatively long segments or for the undeveloped loops which has been observed in 2 vasculatures. System reliability and blood flow in the segment j-k can be increased by additional loops which have been observed in 3 cases.

Numerical calculations of the reflection coefficients in the bifurcations and pressure and flow waveforms $P_j(t,x), Q_j(t,x)$ in the arterial segments have been obtained, where $x \in [0; L_j]$ is the axial coordinate along the segment. The input admittance of the arterial system $Y_{in} = Q_{1,2}(t,0)/P_{1,2}(t,0)$, pressure-flow relationships $P_{1,2}(Q_{1,2})$ and intensities $I^{\pm} = \pm(P \pm \rho c U)^2/(4\rho c)$ of the forward and backward waves where c is the wave velocity have some differences for the vasculatures with different topology. Occlusion of any artery which is situated within the angle AOB (COB) (Figure 7) produces noticeable variations of Y_1 (Y_2) and I_1^- (I_2^-) at insignificant variations of the Y_2 (Y_1) spectrum and I_2^- (I_1^-). When the clamped artery is situated within the angle AOC both the values $Y_{1,2}$ and $I_{1,2}^-$ are changed. The approximate distance to the clamped vessel can be obtained from the dependences $I_{1,2}^{\pm}(t)$.

For the systems with loops localization of the occluded artery (f in Figure 7) is defined by the

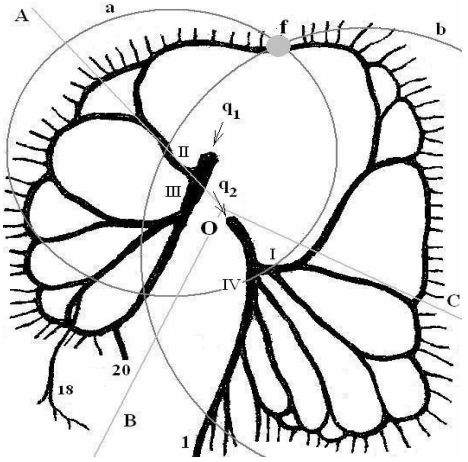

Figure 7: The topological schema of the arterial system of the large intestine

ISSN: 1727-1983

intersection of the circles a,b which radii $r_{1,2}$ can be obtained by calculation the distances $L_{1,2}$ to the reflection cite from $P_1(t), Q_1(t)$ and $P_2(t), Q_2(t)$ curves respectively. The curves can be measured at any cross-section of the feeding arteries by ultrasound devices.

Conclusions

Both the models of branching arterial trees and arterial vasculatures of inner organs possess the so-called resonant harmonics in the amplitude spectra of the input impedances. Any changes in the pulse wave reflections at the terminal elements which characterize normal or pathological state of microcirculation cause noticeable variations of the amplitudes of the resonant harmonics of the given organ and negligibly small variations of the amplitudes of the other harmonics. Individual variations in the diameters and lengths of the vessels within the physiological range produce large quantitative variations of the maximum of the impedance in a narrow frequency range which correspond to the same resonant harmonics. Some discrepancies in the reflection coefficient distribution have been revealed. The reflection coefficient monotonously decreases with increasing the branching order of the tube in the model whereas in the real vasculature Γ_j can change sign at the high branching orders that facilitates blood motion into the small vessels with large hydraulic impedances. The result can be used in clinical applications to pulse diagnostics of the state of the inner organs. The best explanation of the pathological mechanisms is connected with terms excess/deficiency of the oriental medicine.

Parameters of the pulse waves estimated by non-invasively measured pressure and flow curves in the feeding artery of the intraorgan vasculature basing on the developed theory can be used for estimation of the blood flow in the organ and determination of the circulatory disorders at the microcirculatory level.

References

[1] MILNOR, W.R. (1989): 'Hemodynamics, (Williams &Wilkins, Baltimore)
[2] AVOLIO A.P. (1980): 'Multi-branched model of the human arterial system', *Med. Biol. Eng. Comput*., **18**, pp.709-718
[3] KARAMANOGLU M., GALLAGHER D.E., AVOLIO A.P., and O'ROURKE M.F. (1994): 'Functional origin of reflected pressure waves in a multibranched model of the human arterial system', Amer. J. Physiol., **267**, pp.H1681-H1688
[4] JOHN L. R. (2004): "Forward electrical transmission line model of the human arterial system", *Med. Biol. Eng. Comput*., **42**, pp.312–321
[5] KIZILOVA N. A detailed digital model of the human arterial system (2005): 'First Intern. Conf. on Complex Medical Engineering', Proc on CME200. Kagawa, Japan, 2005
[6] BROWN D.J. (1996): 'Input impedance and reflection coefficient in fractal-like models of asymmetrically branching compliant tubes', *IEEE Trans.Biomed.Eng.*, **43**, pp.715-722
[7] BENNETT S.H., GOETZMAN B.W., MILSTEIN J.M., PANNU J.S. (1996): 'Role of arterial design on pulse wave reflection in a fractal pulmonary network', *J.Appl.Physiol*., **80**, pp.1033-1056
[8] BONDARENKO M.Ye., KIZILOVA N.N. (2002): 'Pulse wave reflections in asymmetrically branching arterial networks', *Russian J.Biomech*., **4**, pp.52-62
[9] DAWSON C.A., KRENZ G.S., KARAU K.L. et al (1999): 'Structure-function relationships in the pulmonary arterial tree', *J.Appl.Physiol.,* **86**, pp.569-583
[10] ZAMIR M. (1998): 'Mechanics of blood supply to the heart: wave refection effects in a right coronary artery', *Proc. Royal Soc. London, Ser.B: Biological Sciences*, **265**, pp.439-444
[11] KIZILOVA N.N. (2003): 'Pulse wave reflections in branching arterial networks and pulse diagnosis methods', *J.Chinese Inst. Engineers*, **26**, pp.869-880
[12] KIZILOVA N.N. (2004): Comparative analysis of blood motion in dichotomous branching models of intraorgan vasculature and real arterial beds", Proc. of Euromech Colloquium 456 'Experimental and Computational Biofluid Mechanics', Aachen, Germany, 2004
[13] KIZILOVA N.N. (2004) 'Wave propagation and reflection in systems of compliant tubes', *Intern.J.Fluid Mech.Res*., **31**, pp.608-620
[14] WANG Y.Y., CHANG S.L., WU Y.E. et al (1991): 'Resonance. The missing phenomenon in hemodynamics', *Circul.Res*., **69**, pp.246–249
[15] WANG Y.Y., LIA W.C., HSIU H. et al (2000): 'Effect of length on the fundamental resonance frequency of arterial models having radial dilatation', *IEEE Trans.Biomed.Eng.,* **47**, pp.313-318
[16] YU G.L., WANG Y.L., WANG W.K. (1994): 'Resonance in the kidney system of rats', *Am. J. Physiol.,* **267**, pp.H1544–H1548
[17] TAYLOR M.G. (1966): 'The input impedance of an assembly of randomly branching elastic tubes', *Biophys.J*., **6**, pp.29-51
[18] PARKER K.H., and JONES C.J. (1990): 'Forward and backward running waves in the arteries: analysis using method of characteristics', *J. Biomech. Eng.,* **112**, pp.322-326
[19] HUANG W., YEN R. T., MCLAURINE M. and BLEDSOE, G. (1996): 'Morphometry of the human pulmonary vasculature', *J. Appl.Physiol.,* **81**, pp.2123-2133
[20] ZAMIR M. and PHIPPS S. (1987): 'Morphometric analysis of the distributing vessels of the kidney', *Canad.J. Physiol.Pharmacol.* **65**, pp.2433–2440
[21] Zamir M. and Shee H. (1985): 'Branchimg characteristics of human coronary arteries', *Canad. J. Physiol.Pharmacol,* **64**, pp.661-668
[22] La Barbera M. (1990): 'Principles of design of fluid transport systems in zoology', *Science,* **249**, pp. 992-1000
[23] WANG J.J., PARKER K.H. (2004): 'Wave propagation in a model of the arterial circulation', *J.Biomech.,* **37**, pp. 457-470

ISSN: 1727-1983